High-latitude *E* region ionosphere-thermosphere coupling: A comparative study using in situ and incoherent scatter radar observations

J. K. Burchill,[1] J. H. Clemmons,[2] D. J. Knudsen,[1] M. Larsen,[3] M. J. Nicolls,[4] R. F. Pfaff,[5] D. Rowland,[5] and L. Sangalli[6]

Received 19 September 2011; revised 28 November 2011; accepted 29 November 2011; published 1 February 2012.

[1] We present in situ and ground-based measurements of the ratio κ of ion cyclotron angular frequency to ion-neutral momentum transfer collision frequency to investigate ionosphere-thermosphere (IT) coupling in the auroral *E* region. In situ observations were obtained by NASA sounding rocket 36.234, which was launched into the nightside *E* region ionosphere at 1229 UT on 19 January 2007 from Poker Flat, AK. The payload carried instrumentation to determine ion drift angle and electric field vectors. Neutral winds were measured by triangulating a chemical tracer released from rocket 41.064 launched two minutes later. κ is calculated from the rotation of the ion drift angle relative to the E-cross-B drift direction in a frame co-rotating with the payload. Between the altitudes of 118 km and 130 km κ increases exponentially with a scale height of 9.3 $\pm$ 0.7 km, deviating from an exponential above 130 km. $\kappa = 1$ at an altitude z_0 of 119.9 $\pm$ 0.5 km. The ratio was also estimated from Poker Flat Incoherent Scatter Radar (PFISR) measurements using the rotation of ion velocity with altitude. Exponential fits to the PFISR measurements made during the flight of 41.064 yield $z_0 = 115.9 \pm 1.2$ km and a scale height of 9.1 $\pm$ 1.0 km. Differences between in situ and ground-based measurements show that the *E* region atmospheric densities were structured vertically and/or horizontally on scales of 1 km to 10 km. There were no signs of ionospheric structure in ion density or ion temperature below scales of 1 km. The observations demonstrate the accuracy with which the in situ and PFISR data may be used as probes of IT coupling.

Citation: Burchill, J. K., J. H. Clemmons, D. J. Knudsen, M. Larsen, M. J. Nicolls, R. F. Pfaff, D. Rowland, and L. Sangalli (2012), High-latitude *E* region ionosphere-thermosphere coupling: A comparative study using in situ and incoherent scatter radar observations, *J. Geophys. Res.*, *117*, A02301, doi:10.1029/2011JA017175.

1. Introduction

[2] We present results from a new technique for measuring ionosphere-thermosphere (IT) momentum coupling in the *E* region ionosphere from a spinning spacecraft, and we compare these results with simultaneous observations from an incoherent scatter radar (ISR). Collisional coupling between the ionosphere and neutral atmosphere represents an important pathway for the transport of mass, momentum, and energy in the space environment. Collisions determine where field-aligned currents in the high latitude ionosphere close and thus where magnetospheric energy is deposited [e.g., *Thayer*, 2000]. Numerous satellite observations have indirectly demonstrated that the neutral atmosphere responds to ionospheric forcing at high latitudes, especially in the auroral and magnetic cusp regions [*Emery et al.*, 1985; *Heelis*, 1987; *Knowles et al.*, 2001; *Lühr et al.*, 2004; *Clemmons et al.*, 2008; *Prölss*, 2008; *Sakanoi et al.*, 2009; *Ritter et al.*, 2010]. The resulting variations in neutral density affect low-perigee satellite orbits and consequently impact the accuracy of satellite orbit prediction and tracking operations [e.g., *Storz et al.*, 2005].

[3] Incoherent Scatter Radar (ISR) can probe IT coupling processes [*Dougherty and Farley*, 1963], and many ion-neutral collision frequency estimates have been reported using the ISR technique [e.g., *Reese et al.*, 1991; *Nygren*, 1996; *Davies et al.*, 1997, and references therein]. Equally significant is that ion-neutral collisions play a crucial role in deriving neutral winds, electric current densities, Joule heating rates, and neutral atmospheric properties from ISR measurements [*Alcaydé et al.*, 1972]. In some cases the ion-neutral collision frequency is derived directly from fitting the ISR power spectrum or autocorrelation function to a model,

[1]Department of Physics and Astronomy, University of Calgary, Calgary, Alberta, Canada.
[2]Space Science Applications Laboratory, The Aerospace Corporation, El Segundo, California, USA.
[3]Department of Physics and Astronomy, Clemson University, Clemson, South Carolina, USA.
[4]Center for Geospace Studies, SRI International, Menlo Park, California, USA.
[5]NASA Goddard Space Flight Center, Greenbelt, Maryland, USA.
[6]Department of Physics, Royal Military College of Canada, Kingston, Ontario, Canada.

0148-0227/12/2011JA017175

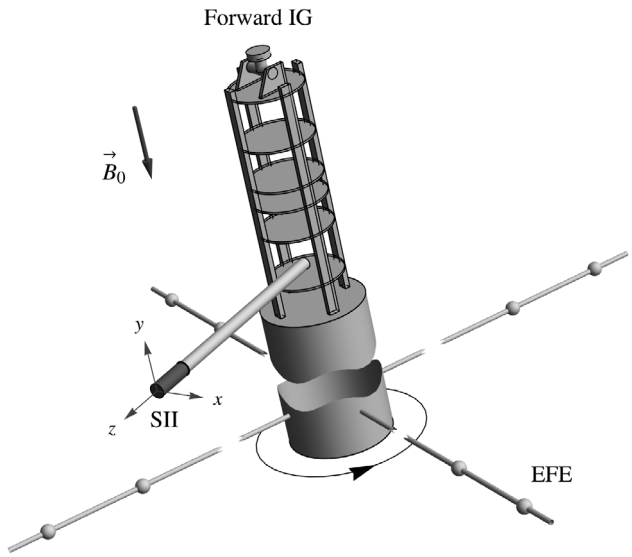

Figure 1. Illustration of 36.234 experiment payload (not to scale) showing the Suprathermal Ion Imager (SII) and its coordinate system, the forward Ionization Gauge (IG), and the Electric Field Experiment (EFE) booms. (The payload bus and EFE booms have been foreshortened for the purpose of illustration.) The payload symmetry axis was aligned to within a few degrees of the geomagnetic field vector ($\vec{B}_0$) by an attitude control system. The payload spin period was 1.6 s.

which typically involves assuming the ion and electron temperatures are equal and/or equal to the neutral temperature. An alternative technique uses measurements of the altitude variation of ion drifts [e.g., *Nygren et al.*, 1987, 1989; *Davies et al.*, 1997]: Ions transition from drifting with the neutrals at low altitudes (collisional regime) to drifting at the $\mathbf{E} \times \mathbf{B}$ velocity at high altitudes (collisionless regime). As the neutral winds usually are not measured, this method typically assumes they are negligible. Uncertainty about the validity of the assumptions that go into each technique makes automation difficult. So, despite substantial progress in this area, collision frequencies usually are not quoted in ISR observations. Combining ISR measurements with simultaneous in situ observations provides a means of examining and validating those assumptions, and this is one element of our study.

[4] In contrast to the many ground-based observations cited above, only two direct in situ observations of ion-neutral coupling in the *E* region have been reported in the literature. The pioneering study by *Watanabe et al.* [1991] used sounding rocket observations to demonstrate ion demagnetization in the *E* region ionosphere, although neutral winds were not measured. Progress was made recently by *Sangalli et al.* [2009] who used ion drift, electric field, and neutral wind measurements obtained by a pair of sounding rockets from the Joule-II campaign to self-consistently estimate the height z_0 of the boundary between collisional and collisionless ion drift to be 118.0 ± 0.3 km during an auroral breakup near Poker Flat, AK, on 19 January 2007.

[5] In this paper we analyze ion drift, electric field, and neutral wind measurements obtained by a second pair of rockets (36.234 and 41.064) from the Joule-II mission, during the same auroral breakup, and derive a height profile for the ratio κ of ion cyclotron frequency to ion-neutral momentum transfer collision frequency. We validate the in situ results by comparing scale heights in κ with neutral atmosphere pressure scale heights measured by an ionization gauge. We then compare these measurements, and those of *Sangalli et al.* [2009], with measurements from the Poker Flat Incoherent Scatter Radar (PFISR) to assess the accuracy of the radar observations of IT coupling. The instruments and observations are described in section 2. Section 3 presents the techniques and results, which are discussed and summarized in section 4. Appendix A provides details on both the error analysis and the ion-neutral momentum transfer collision frequency model calculations.

2. Instrumentation and Data

[6] NASA sounding rocket 36.234 was part of the Joule II mission to study frictional heating in the *E* region ionosphere [*Sangalli et al.*, 2009; *Hysell et al.*, 2008]. The rocket launched from the Poker Flat Research Range at 1229 UT on 19 January 2007 during a period of relative calm in both the aurora (quiet, stable arc) and geomagnetic activity ($K_p \sim 2+$ to $3-$, $a_p \sim 10$ nT, and DST ~ -10 to -15 nT in the hours surrounding the launch). An attitude control system (ACS) was used to orient the payload rotational axis to within a few degrees of the local geomagnetic field direction and to maintain the payload spin period at 1.6 s. The payload carried multiple instruments to an altitude of 190.2 km, including a Suprathermal Ion Imager (SII), which takes snapshots of the ion energy/arrival angle probability distribution function at a rate of 125 distributions per second. The SII was mounted at the end of a 1 m boom on the rocket payload as illustrated in Figure 1. Details related to the SII principle of operation are given by *Knudsen et al.* [2003]. Of relevance to the present study is that the SII analyzer projects an image of the differential directional energy flux of ions arriving within $\pm 5°$ of the plane of its cylindrical entrance aperture onto a microchannel plate intensifier (Figure 2). Because the payload spins about its symmetry axis (see Figure 1), the total detector counts are modulated as the entrance aperture sweeps across the ion ram direction. There is a peak in number of ions entering the aperture when the ram vector lies within the aperture field of view. On this flight there was a fracture in the MCP detector which precluded obtaining estimates of the ion velocity vector. As will be shown in section 3, we estimate the direction of the ion flow vector by determining the relative spin phase at which the integrated ion flux is a maximum. See *Drakou et al.* [1997] and *Knudsen and Wahlund* [1998] for other applications that use the total flux from a spinning probe to determine plasma properties. Figure 3 shows an ion distribution image that is representative of the data obtained on this flight. It is evident from watching a movie of the image time series that the MCP intensifier is cracked, and this distorts the distribution of signal within the image. Therefore we have selected for analysis the lower-right hand side of each image, where the MCP is operating nominally. The selected data correspond to altitudes below 155 km on the descent stage of the rocket's trajectory. The circular fiducials represent kinetic energies of 2 eV and 5 eV, assuming singly

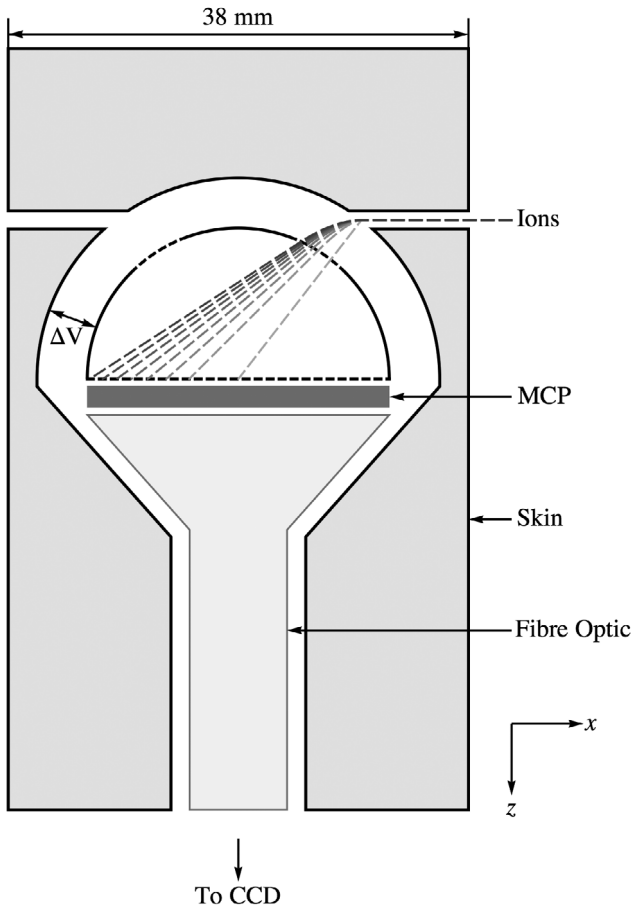

Figure 2. Illustration of the Suprathermal Ion Imager principle of operation. Figure 2 represents a 2D section in the *x*-*z* plane of the coordinate system in Figure 1. After *Burchill et al.* [2010].

ionized ions. A bias of −1.9 V relative to payload ground was applied to the sensor skin, and the peak signal lies just outside the inner fiducial, consistent with a slightly negative payload floating potential. The integration period for the ion distribution images is 8 ms.

[7] Rocket 36.234 also carried a multiple-sensor ionization gauge in order to measure the state of the ambient thermospheric gas. This instrumentation consists of five pressure sensors oriented such that the ambient flow is sampled at five angles of attack. The sensors employ miniature Bayard-Alpert ionization gauges [*Bayard and Alpert*, 1950] and modern, high dynamic-range electrometers for sensitive pressure measurements. Each gauge measures the pressure inside its own accommodation chamber. One sensor, the forward sensor, was located on the forward payload deck and oriented with its entrance aperture normal aligned with the spin axis. The purpose of this sensor was to enable temperature and density profiles to be determined via the standard "hypsometric" method [e.g., *Horowitz and LaGow*, 1957]. For this study, we use the neutral pressure measurements on the upleg to validate the κ scale height measurements.

[8] The DC and AC vector electric fields were measured using spherical sensors with embedded pre-amps extended on 5.2 m tip-to-tip articulated fiberglass booms that unfolded after the payload had attained sufficient altitude in the lower ionosphere. Since the payload spin axis was oriented along the magnetic field direction, the two-dimensional electric field measurement completely parameterized the electric fields perpendicular to the magnetic field direction. The DC electric field data were sampled with 18 bit A/D converters with a time resolution of 1 msec. The $\vec{v}_{\text{payload}} \times \vec{B}$ fields were subtracted from the measurements and the resulting DC electric fields were then rotated into geomagnetic coordinates using the attitude solutions provided by the on-board gyroscope. Electric field data gathered during this flight are analyzed and discussed by *Hysell et al.* [2008]. Data used for the present analysis were obtained from fits of one component at twice per spin (1.25 Hz) to reduce measurement noise.

[9] A second rocket (41.064) launched at 1231 UT released a luminescent tracer (trimethyl aluminate) which was triangulated optically by ground stations to determine the zonal and meridional components of the neutral bulk velocity vector. In the following analysis we use data from the upleg of 41.064, as measurements were not available from the downleg.

[10] The in situ measurements were complemented by ionospheric observations from the Poker Flat Incoherent Scatter Radar (PFISR) facility. PFISR operated in a mode with seven beams, as illustrated in Figure 4 and described by *Heinselman and Nicolls* [2008] and *Hysell et al.* [2008, 2009]. PFISR transmissions consisted of interleaved long pulses and alternating codes. The long pulse and alternating code data were integrated for two and five minutes, respectively, prior to performing incoherent spectral analysis. The multibeam, pulse-to-pulse steering capability of PFISR

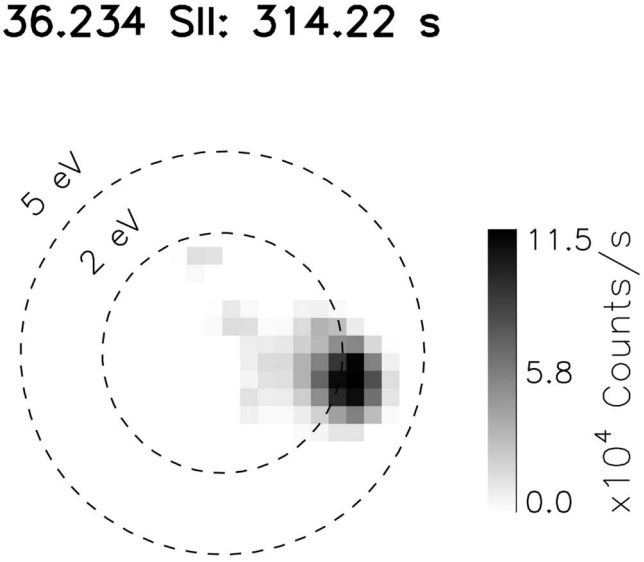

Figure 3. Representative ion image at T + 294.36 s. The dashed circular fiducials represent kinetic energies 2 eV and 5 eV, assuming singly ionized particles. Pixel count rate is represented linearly by the gray scale. The signal peak lies slightly outside of the 2 eV circle. This is consistent with negative payload charging of a fraction of a volt relative to the plasma.

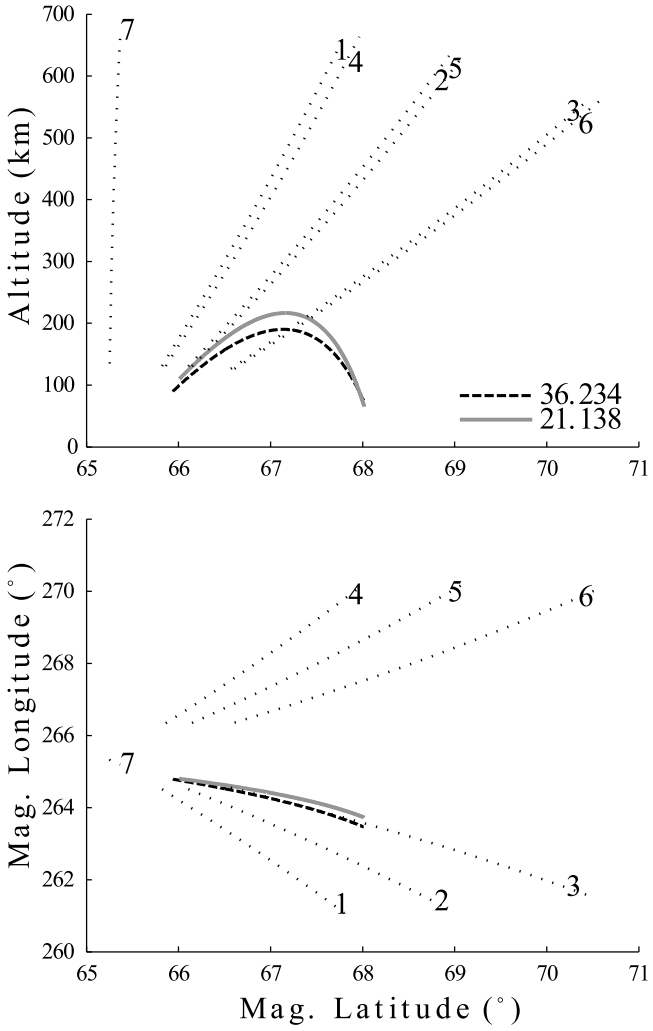

Figure 4. PFISR beam geometry and rocket trajectories in altitude-adjusted corrected geomagnetic coordinates. (bottom) Magnetic longitude vs. magnetic latitude and (top) altitude vs. magnetic latitude. The radar beams (dotted lines) are numbered 1 through 7, and beam 7 points anti-parallel to the geomagnetic field line. Curves denote sounding rockets 36.234 (dashed) and 21.138 (solid).

allows vector drifts, and corresponding inferred electric fields and neutral motions, to be derived.

3. Techniques and Results

[11] Under the steady state guiding center approximation, ions drift with the average velocity $\vec{v}_{i\perp}$ in the direction perpendicular to the geomagnetic field vector according to

$$\vec{v}_{i\perp} = \frac{1}{1+\kappa^2}\vec{u}_\perp + \frac{\kappa}{1+\kappa^2}\left(\vec{E}_\perp/B + \vec{u}_\perp \times \hat{b}\right) + \frac{\kappa^2}{1+\kappa^2}\vec{E}_\perp \times \hat{b}/B, \quad (1)$$

where $\kappa = \Omega_i/\nu_{in}$ is the ratio of the average ion cyclotron angular frequency to the average ion-neutral momentum transfer collision frequency, $\vec{E}$ is the electric field vector, B and $\hat{b}$ are the magnitude and direction of the geomagnetic field, and $\vec{u}$ is the average drift velocity of the neutral atmosphere. Equation (1) is a special case of equation (5.103) of *Schunk and Nagy* [2009], for which ion pressure gradients and gravity are negligible. All neutral species are assumed to drift with the same velocity, as are all ion species. In what follows we describe how equation (1) is used to determine κ from the in situ measurements, and describe a method to estimate the effect of collisions using ISR observations.

3.1. In Situ Method and Results

3.1.1. Ion Ram Demagnetization

[12] *Sangalli et al.* [2009] calculated κ from the ratio $|\vec{v}_{i\perp} - \vec{u}_\perp|/|\vec{E}_\perp/B - \vec{v}_{i\perp} \times \hat{b}|$ (see equation (1)) using measurements of the electric and magnetic fields, the ion drift, and the neutral wind from rockets 21.138 and 41.065. In the absence of vector ion drift measurements on 36.234, we solve equation (1) for $\vec{v}_{i\perp}$ to calculate the deflection θ of the ion ram vector due to ion-neutral collisions assuming a particular value of κ, and find that κ for which the calculated deflection matches the observed deflection. Figure 5 illustrates the geometry of the calculation. From measurements of the payload velocity ($\vec{v}_{p\perp}$), the neutral velocity ($\vec{u}_\perp$), and the electric field ($\vec{E}_\perp$), we calculate the ion velocity for each of a set of κ values running from $10^{-1.500}$ to $10^{1.500}$ in factors of $10^{0.001}$. From these we calculate the expected angle θ

$$\theta = \arccos\left(\frac{\vec{v}'_{i\perp} \cdot \vec{v}'_{E\times B}}{|\vec{v}'_{i\perp}||\vec{v}'_{E\times B}|}\right) \quad (2)$$

between the observed ion ram vector $\vec{v}'_{i\perp} = \vec{v}_{i\perp} - \vec{v}_{p\perp}$ (ram) and the rammed E-cross-B drift vector $\vec{v}'_{E\times B} = \vec{v}_{E\times B} - \vec{v}_{p\perp}$ in the frame of reference co-rotating with the spinning payload. As seen in the payload frame, nonzero values of θ represent a "demagnetization" of the ion ram vector due to collisions with neutrals. The true κ is obtained where θ matches the observed deflection angle, θ_m. We perform the calculations in a plane perpendicular to the magnetic field vector calculated from the eleventh generation International Geomagnetic Reference Field model [*Finlay et al.*, 2010].

[13] Figure 6a shows a representative time series of the SII count rate obtained from a sum over the right half of the SII images. Figures 6b–6d show selected spin profiles with four-parameter Gaussian fits (dashed curves) at three different altitudes of the rocket. The gray curves in each panel are components of the $\vec{v}'_{E\times B}$ projected onto the SII entrance aperture. The time difference Δt between the peak in the SII signal and the peak in the projection of $\vec{v}'_{E\times B}$ is converted to a ram deflection angle (the angle between the ion drift vector and the $\vec{E} \times \vec{B}$ vector in the payload frame of reference) according to

$$\theta_m = (\Delta t/T) \times 360° \quad (3)$$

where $T = 1.6$ s is the spin period of the payload. We use the fact that $\theta_m = 0°$ above 140 km to calibrate the angle between the SII boom and the electric field x-axis to within 0.25°. Figure 6a is the count rate profile at an altitude of ~149 km, where the ions are E-cross-B drifting. Figure 6c shows the profile measured at ~125 km, showing a clear demagnetization of the ion ram vector. The E-cross-B drift can either lead (as shown) or lag the SII signal, depending on the relationship between $\vec{E}_\perp$, $\vec{v}_{p\perp}$, and $\vec{u}_\perp$. Figure 6c

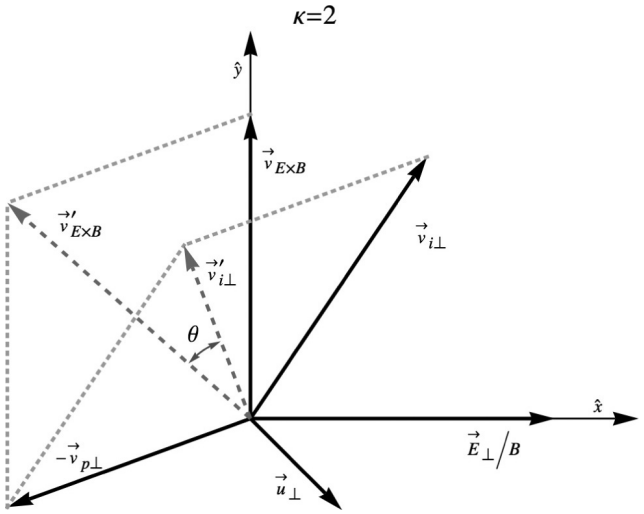

Figure 5. Illustration of deflection of ion ram vector due to ion-neutral collisions ("ion ram demagnetization"). From measurements of the payload velocity ($\vec{v}_p$), the neutral velocity ($\vec{u}_\perp$), and the electric field ($\vec{E}_\perp$), we calculate the expected angle θ between the observed ram vector $\vec{v}'_\perp$ and the E-cross-B vector $\vec{v}'_{E\times B}$ for a range of κ values. We obtain the true κ where θ matches the observed deflection angle, θ_{measured}.

again shows significant demagnetization, at an altitude of ~110 km.

[14] Figure 7 shows the altitude profile of the measured deflection angles. Between 140 km and 150 km the standard deviation of the deflection angle is 0.25°, and we use this as an estimate of the uncertainty in the deflection angle measurement, $\Delta\theta_{\text{m}}$.

[15] We use the calibrated ram deflection measurements between 118 km and 140 km to determine κ according to the technique described above. Analysis of the uncertainties in κ are presented in section A1. The angular deflection is anomalously large for the observed neutral wind and electric field at altitudes below 117 km, and we are unable to obtain measurements of κ in that region. Figure 8 shows the resulting height profiles of κ and ν_{in} between 118 km and 140 km. To identify the height z_0 at which the ion-neutral momentum transfer collision frequency matches the ion cyclotron angular frequency, we fit a straight line to the model

$$\ln\kappa = (z - z_0)/H_\kappa, \tag{4}$$

over the height range 117–131 km where the profile is approximately exponential. The result is the straight line in Figure 8a, where $z_0 = 119.9 \pm 0.5$ km and the corresponding κ scale height is $H_\kappa = 9.3 \pm 0.7$ km. For comparison we have calculated the theoretical ion-neutral collision frequency (dashed curve) for model neutral densities from NRL-MSISE-00 [*Picone et al.*, 2002] and IRI 2007 [*Bilitza and Reinisch*, 2008] using non-resonant polarization attraction interactions as described by *Schunk and Nagy* [2009]. Further information about this calculation is provided in section A2. Using IRI for the mean ion mass, we derive ν_{in} as shown in Figure 8b, which fits an exponential model with a scale height of 9.3 ± 0.7 km and a collision frequency of 170 ± 10 s^{-1} at 119.9 km. We emphasize that the data points in Figure 8a are from observations only, whereas the data points in Figure 8b are derived in part from the IRI mass height-profile.

3.1.2. Validation of in Situ Measurements

[16] Since the ion-neutral collision frequency is proportional to neutral density, the κ scale height H_κ is a good approximation for the neutral density scale height over small ranges of altitude. To estimate the height variation of H_κ, we performed least squares fits of the exponential model to successive pairs of κ measurements between 117 km and 131 km, the region over which κ varies approximately exponentially. Results are shown in Figure 9 which includes the NRL-MSISE-00 model scale height (dashed line) calculated

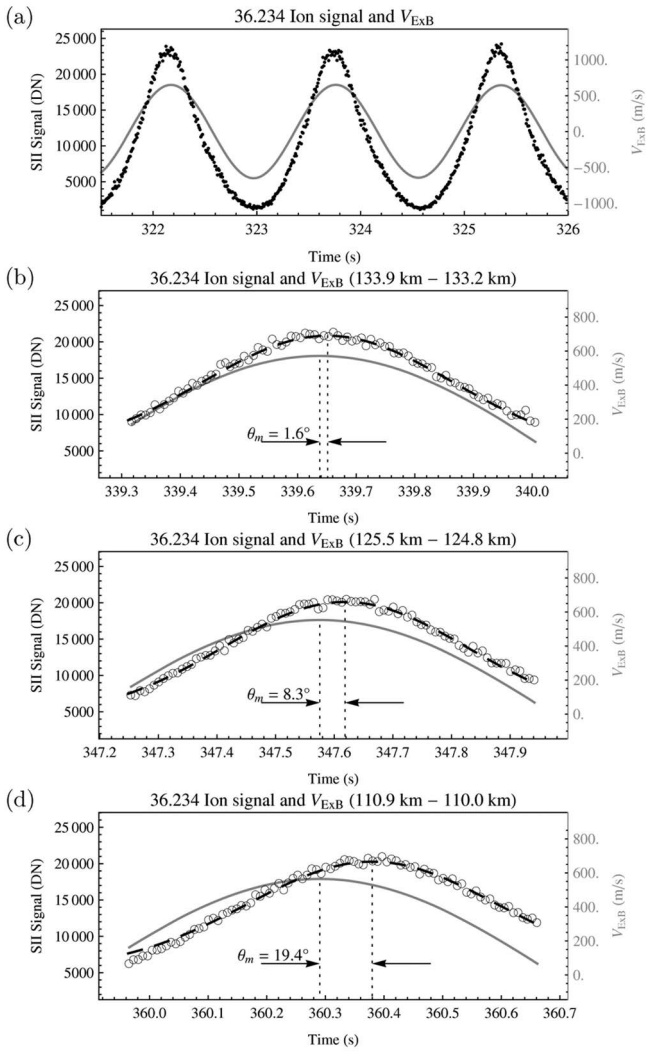

Figure 6. Time series plots of total SII signal, with four-parameter Gaussian fits (dashed curves). The gray curve in each panel is the component of the E-cross-B drift velocity projected into the plane of the SII aperture. The labeled arrows show the equivalent phase shifts between the SII signal and the E-cross-B drift in the rammed payload frame. (a) An example of the profiles used for calibrating the E-cross-B direction and the measurement uncertainty. (b and c) Zoomed examples from the profiles used to calculate κ. (d) An example profile for which equation (1) has no solution.

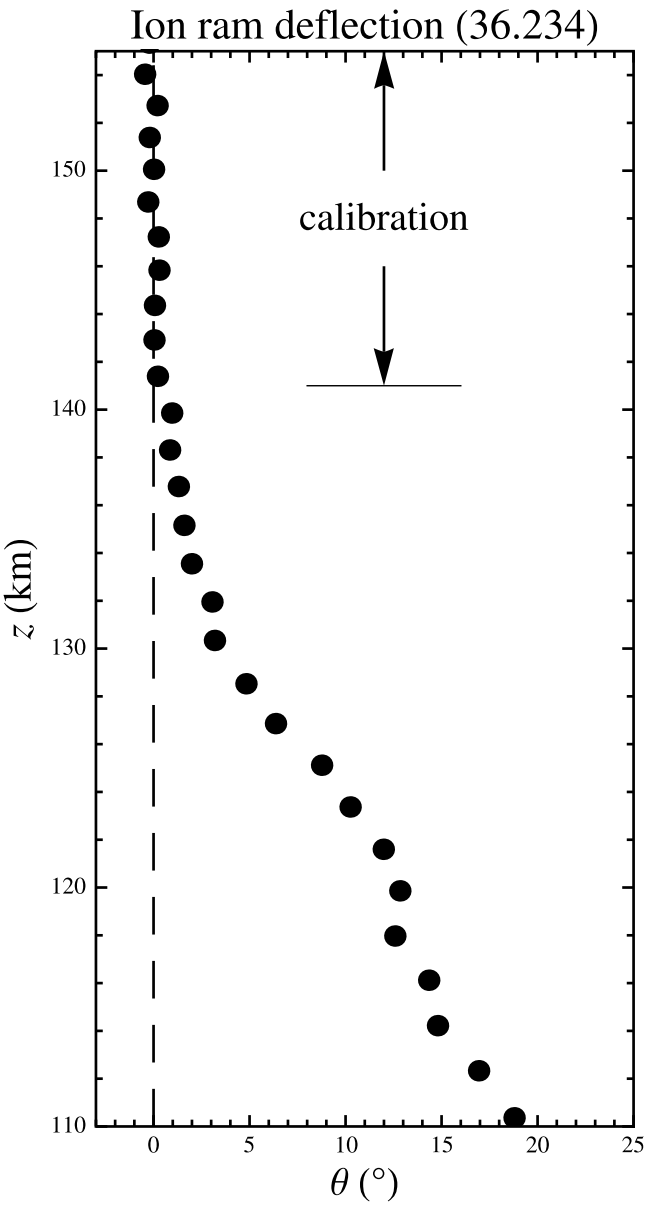

Figure 7. Angular deflection of ion ram vector ($\vec{v}_{\perp}^{'}$) from the E-cross-B vector ($\vec{v}_{E\times B}^{'}$) as observed in the payload reference frame. Below 117 km the measured angular deflection is anomalously large and we are unable to obtain estimates for κ below this altitude.

along the rocket trajectory for reference. Neutral atmospheric pressure scale heights (solid line) calculated from the ionization gauge measurements, using MSIS for the neutral composition, are also shown. The scale-heights derived from the SII ion ram deflection agree very well with ionization gauge (IG) neutral scale height measurements below 125 km, providing a convincing validation of the κ measurements in this region.

3.2. PFISR Method and Results

[17] Typically, incoherent scatter spectra or autocorrelation functions are fit for electron and ion temperatures (as well as other parameters, like Doppler motion and electron density) under the assumptions of a composition profile and a collision frequency. In the lower *E* region (90–100 km), the plasma is collisional and it is reasonable to assume that electron and ion heating are negligible and that the plasma is in thermal equilibrium with the neutrals. In this collisional regime, the ISR spectrum becomes Lorentzian in shape [e.g., *Dougherty and Farley*, 1963] and the correlation time (inverse of spectral width) is proportional to νT^{-1}, where ν is the momentum transfer collision frequency and T is the temperature. Thus a spectral change is ambiguous in terms of a change in collision frequency and temperature. For the purposes of IS fitting, this ambiguity makes it impossible to fit for temperature and collision frequency at the lower *E* region altitudes. At slightly higher altitudes, it may be possible to fit for collision frequency and temperature simultaneously, however one must be cautious of the breakdown in assumptions about thermal equilibrium as the ions are heated by frictional heating and the electrons are heated by wave-particle interactions [e.g., *St.-Maurice et al.*, 1981; *Hysell et al.*, 2009].

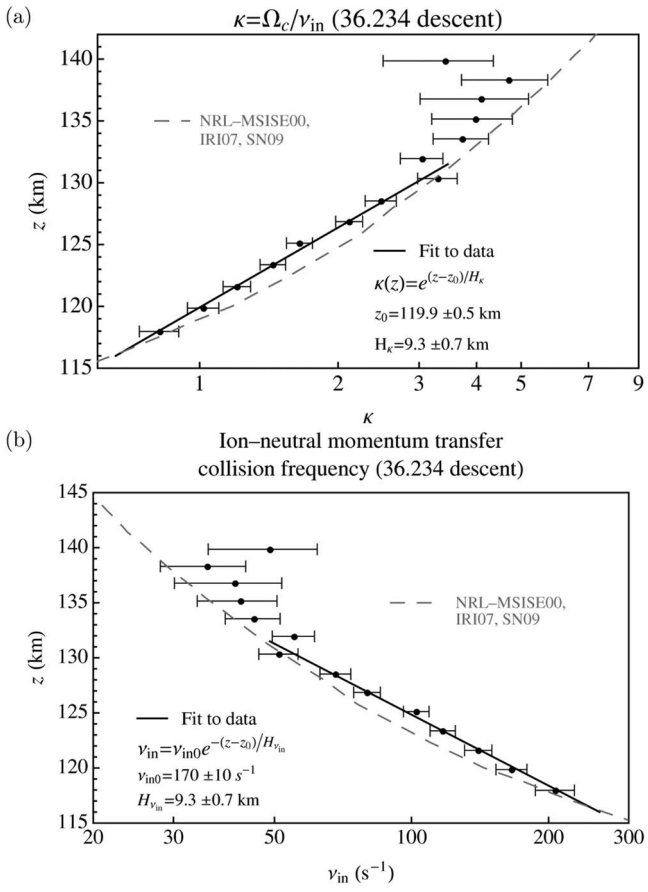

Figure 8. Height profiles of (a) κ, the ratio of ion cyclotron angular frequency to ion-neutral momentum transfer collision frequency ν_{in}, and (b) the ion-neutral moment transfer collision frequency. The solid curves are least squares fits to exponential models. The long-dashed curves are the theoretical results calculated according to the prescription in section A2. In Figure 8a, the data points are calculated from observations only, whereas in Figure 8b the data points are derived from the observed κ using the IRI model for the mean ion mass.

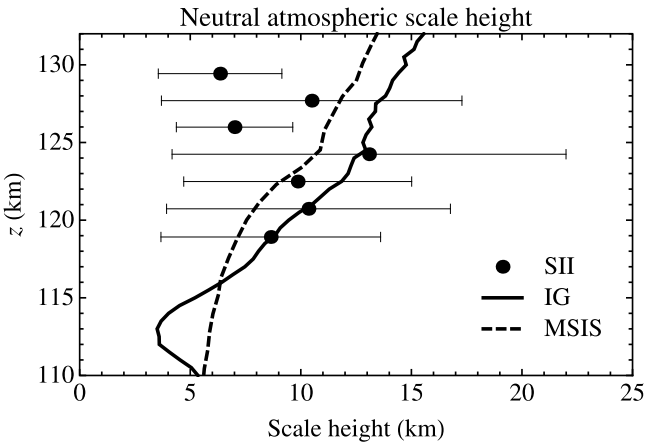

Figure 9. Height profile of the neutral density scale height derived from measurements of neutral temperature (solid line) and measurements of the κ scale height (points). Also plotted is the MSISE-00 neutral scale height (dashed line) for rocket 36.234.

[18] An alternative technique is based on measurements of the variation of ion velocity with height, using equation (1) to obtain κ. This approach is similar to the analysis of the rocket data, except that in this case the full ion velocity drift vector perpendicular to the magnetic field is measured, and there is no independent measurement of electric field. To obtain κ we 1) resolve line-of-sight velocity into a vector as a function of altitude; 2) determine the $\vec{E} \times \vec{B}$ drift from data at altitudes greater than 200 km; and 3) solve equation (1) for κ as a function of altitude using the same approach as *Sangalli et al.* [2009], with and without the inclusion of the neutral winds measured by the rocket. Individual measurements are resolved at 5-minute resolution over two 15-min intervals, centered on the two TMA rocket launches: 12:24:54–12:40:13 and 12:40:14–12:55:32. We estimate κ from the mean of those three measurements, and estimate the uncertainties as the standard deviation over $\sqrt{3}$. The data and results are shown in Figure 10. Shown are observations and results derived using winds from TMA rocket 41.064 launched at 1231 UT (Figure 10, top) and TMA rocket 41.065 launched at 1246 UT (Figure 10, bottom). Figure 10 (left) shows vector winds (smooth curves), smoothed over 8 km, and ion velocities (points) in geomagnetic coordinates, where black is East and gray is North. Figure 10 (right) shows κ derived with (black) and without (gray) the neutral wind taken into account. Least squares fits (dashed lines) using equation (4) give z_0 = 115.9 ± 1.2 km (top) and z_0 = 119.9 ± 1.1 km (bottom), with scale heights of 9.1 ± 1.0 and 7.3 ± 0.9 km, respectively.

[19] Figure 11a compares the in situ measurements from rocket 36.234 (dots) with those from the PFISR calculated from averages over the interval 12:24:54 UT to 12:40:13 UT (squares). Figure 11b compares the in situ measurements of *Sangalli et al.* [2009] with those of PFISR averaged over the interval 12:40:14 UT to 12:55:32 UT.

4. Discussion

[20] The smoothness of the ion signal within a payload spin period suggests that there is very little structure in either the ion density or ion temperature over the course of a payload spin period, which corresponds to spatial scales less than 1 km. Large electric fields were observed on the upleg portion of 36.234, but the downleg had field strengths less than 5 mV/m, consistent with $T_i - T_n < 20$ K [*Saint-Maurice and Hanson*, 1982], assuming that there are not significant wave-particle interactions. This validates one of the key assumptions that goes into the analysis of PFISR spectra in this altitude region, at least for this case study.

[21] Often it must be assumed that neutral winds are negligible when estimating collision frequencies from ISR data. In our case study, comparison of the PFISR κ profiles that are calculated with and without neutral winds is consistent with previous work [e.g., *Thayer*, 2000] that shows ignoring neutral winds can introduce significant errors on estimates of κ (and hence collision frequency) in the transition region.

[22] Another assumption that goes into the analysis of low-altitude PFISR data is that the ionosphere is homogeneous and static over scales and times sampled by the radar beams. In situ observations can provide insight into the validity of this assumption for the event studied here. During the first interval (Figure 8), between altitudes of 118 km and 128 km, the in situ measurements show a 20% decrease in κ relative to the empirical model. This difference is consistent with a local enhancement in neutral density relative to the model. This observation provides evidence for localized Joule heating below 125 km causing a localized vertical (and/or horizontal) structuring of neutral mass density over scales of a few km. The in situ observation of z_0 reported here is 1.9 km higher than that reported by *Sangalli et al.* [2009] for the period approximately 16 min later, and 4 km higher than that obtained by the radar. In the case of the two in situ measurements, the difference cannot be explained by the reported measurement uncertainties, so it is due either to unaccounted-for systematic errors in one or both of the measurements, or it is a true difference. Due to the exponential falloff in neutral density with height, a difference of 1.9 km in z_0 represents a significant variation in neutral atmospheric structure. Also significant is the large difference in the atmospheric scale height obtained from these two rockets. Examination of *Sangalli et al.* [2009, Figure 8] reveals a relatively constant scale height of about 5 km in the range 108 km to 128 km, about half the value reported here. The two rocket flights were 16 min apart and their lateral separation was approximately 11 km at a height of 120 km on their descents (see Figure 4). There is an excellent agreement between the radar and in situ κ measurements for the second interval (rocket 21.138) over a limited height range of 108–118 km (Figure 11b). There are significant differences outside this altitude range, and the in situ estimate for z_0 during the second interval (119.9 ± 1.1 km) does not agree with the in situ estimate from *Sangalli et al.* [2009] (118.0 ± 0.3 km) at the 1-sigma uncertainty level. Piecing these observations together paints a picture of an atmospheric neutral density that is structured at scales of 1–10 km, vertically and/or horizontally, and that is also changing in time. This structure might explain some of the differences between the radar and in situ observations, since the radar measurements are averaged over larger distances (on the order of several km horizontally) and longer times (averages of three five-minute integrations). Notwithstanding this qualification, incoherent scatter radars can provide accurate measurements of IT coupling. We note the excellent agreement between

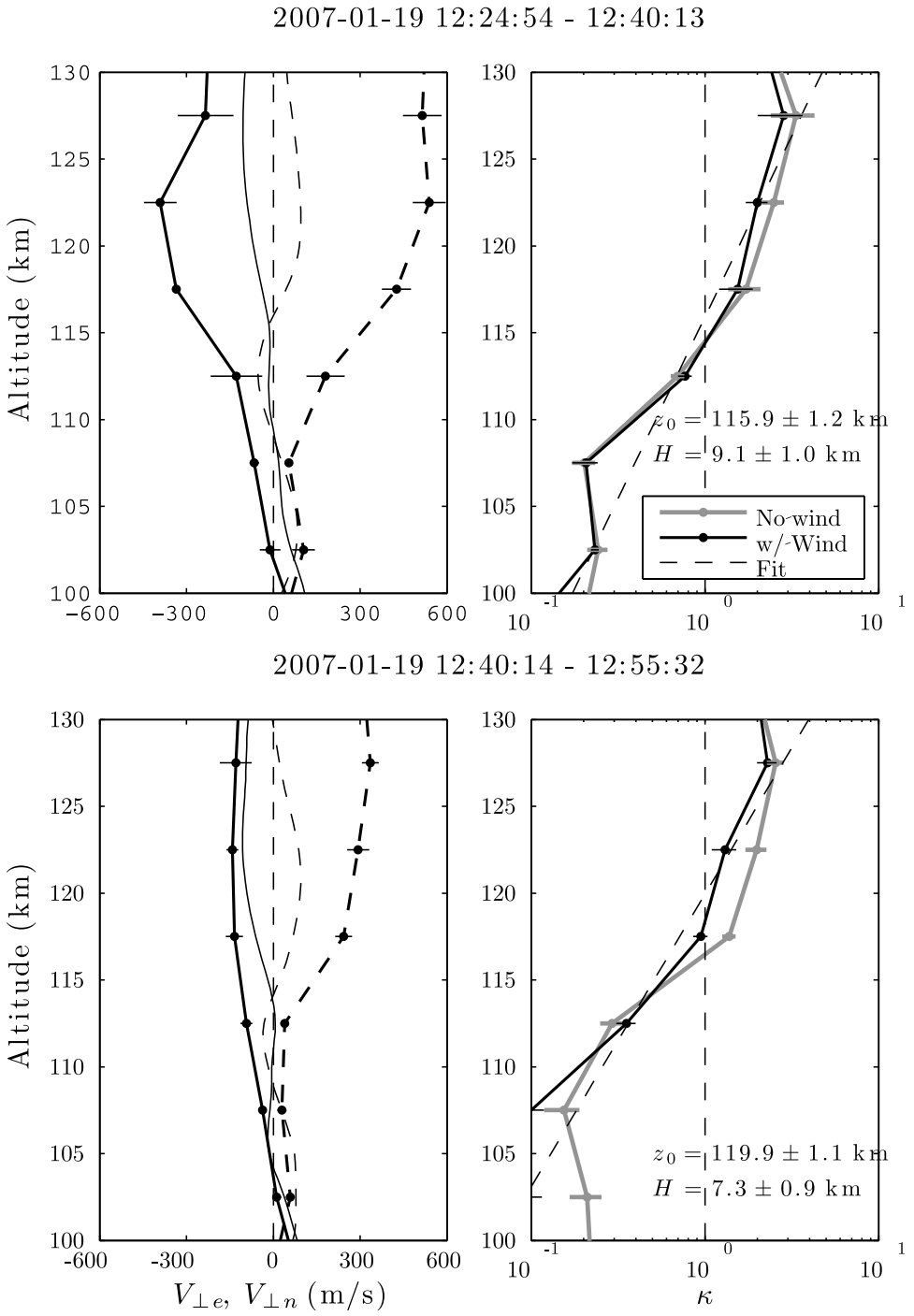

Figure 10. Determination of κ from PFISR observations. Shown are observations and results derived from two 15-minute intervals centered on the TMA rocket launches: (top) TMA rocket 41.064 launched at 1231 UT and (bottom) TMA rocket 41.065 launched at 1246 UT. (left) Vector velocities of winds (smooth curves) and ions (segmented curves), where black is East and gray is North. (right) κ derived with (black) and without (gray) the neutral wind taken into account.

κ scale height measurements made in situ (9.3 ± 0.7 km) and with the radar (9.1 ± 1.0 km) during the first interval.

[23] Above 118 km the technique for determining κ from a spinning spacecraft is robust since few assumptions go into the measurement. We have seen with rocket 36.234 that accurate estimates of the collision frequency based on deviations of the ion drift angle relative to the E-cross-B drift direction are only possible with precise calibration of the relative angle between the measurements to an accuracy of 0.25°. This calibration takes into account misalignments of instrumentation and other sources of error. The results are insensitive to variations in spacecraft charging, which can affect measurements based on the magnitude of the ion velocity if not accurately accounted for. Moreover, there is

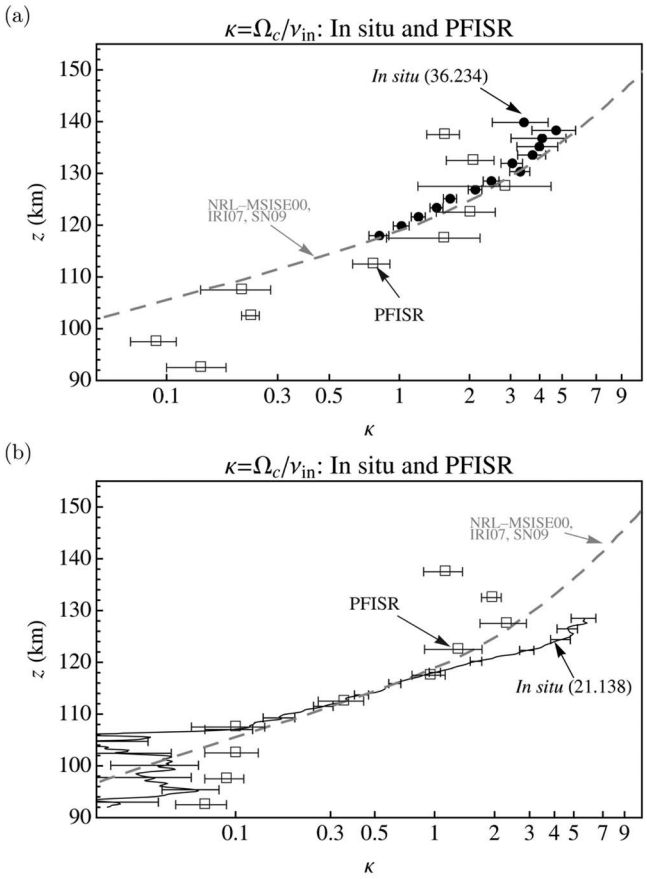

Figure 11. (a) Comparison of in situ (circles) and PFISR (squares) measurements of κ obtained during the flights of the first pair of rockets 36.234 and 41.064. (b) Comparison of in situ (solid line) and PFISR (squares) for the period covering the second pair of rockets 21.138 and 41.065. The solid curve in Figure 11b, from rocket 21.138, is the data of *Sangalli et al.* [2009].

no assumption about the form of the ion velocity distribution function. In principle the in situ technique does not require calibration against electric field measurements when the angular position of the SII and electric field booms is known with sufficient accuracy and precision. Future experiments could be conducted using precision boom angle measurements to eliminate the need to calibrate the ion measurement in the region above 140 km. Variability in ion density and/or ion temperature within a payload spin period would, however, reduce the effectiveness of the technique.

[24] Below 118 km the deflection of the ion ram vector on rocket 36.234 is significantly larger than what is expected from the observed neutral wind and electric field observations. An explanation may lie in the fact that the neutral wind measurements were obtained from the upleg of rocket 41.064, whereas the ion and electric field measurements were obtained on the downleg of rocket 36.234. Any variations in winds between the two times and different latitudes could affect the κ estimates particularly at lower altitudes, where the ion drift is largely controlled by the neutral atmosphere.

[25] *Watanabe et al.* [1991] presented observations from three rockets of the ratio of ν_{in}/Ω_i based on measurements of $\vec{v}_{i\perp}$, $\vec{E}_\perp$, and $\vec{B}$, with the assumption that $\vec{u}_\perp = 0$, and found that above 125 km under quiet auroral conditions the ions drift according to

$$\vec{v}_{i\perp} = \vec{E}_\perp \times \hat{b}/B \tag{5}$$

to a good approximation. Our in situ observations, from the downleg of rocket 36.234, were obtained from the north side of a weak auroral arc, and the weak electric fields on the downleg (<5 mV/m) are consistent with a quiet auroral environment. Deviations from the E-cross-B drift approximation equation (5) are evident in Figure 7 at altitudes up to 140 km, and show precisely at what altitude the approximation can begin to break down under quiet auroral and geomagnetic conditions. *Watanabe et al.* [1991] used the assumption $\vec{u}_\perp = 0$ and the measured scale height H and ratio ν_{in}/Ω_i above 115 km to estimate the neutral wind altitude profile below 115 km assuming an exponential model for the collision frequency. For the present case, the MSIS and IRI models show that the collision frequency does not vary exactly exponentially over scales greater than a few km in this atmospheric transition region, but the observations from rocket 36.234 reveal that an exponential model for collision frequency appears to work well between 118 km and 130 km in this case. But as we do not have full ion velocity vector information from 36.234, we are unfortunately unable to estimate the neutral winds using the method of *Watanabe et al.* [1991], independently of the TMA measurements.

[26] If the results from rocket 36.234 are taken as representative of quiet auroral conditions, we see that qualitatively the MSIS and IRI models do well in representing collision frequencies, but also that there are disparities between the empirical models and observations over scales of 1–10 km. Figures 8 and 9 show that, to within measurement uncertainties, the κ scale height is approximately constant through the altitude region 118–130 km. Given that the neutral atmosphere is not isothermal in altitude, there is evidence that details of either or both of the average neutral particle and ion mass height profiles are not represented accurately at scales of 1–10 km by the MSIS and IRI models. These points serve as a reminder that the empirical models should be used with caution when applied to problems over scales of 1–10 km, even under quiet auroral conditions.

5. Conclusions

[27] 1. This study presents a treatment and analysis of in situ (NASA rockets 36.234 and 41.064) and incoherent scatter radar (PFISR) measurements to investigate ion-neutral momentum coupling of the high-latitude auroral ionosphere-thermosphere system.

[28] 2. We have introduced a robust technique for estimating ion demagnetization in the *E* region ionosphere from an ion analyzer and an electric field antenna on a spinning spacecraft (Figures 6 and 7).

[29] 3. Ion velocity and electric field measurements were combined with neutral wind measurements to estimate the height profile of $\kappa = \Omega_i/\nu_{in}$ between 118 km and 140 km (Figure 8) in a relatively undisturbed auroral *E* region.

[30] 4. During the period 12:24:54 UT to 12:40:13 UT, the height of transition between the collisional and collisionless regimes (for which $\kappa = \Omega_i/\nu_{in} = 1$) was measured in situ to be

z_0 = 119.9 ± 0.5 km (Figure 8), and by PFISR to be z_0 = 115.9 ± 1.2 km (Figure 10). The scale height measurements were in excellent agreement: 9.3 ± 0.7 km (in situ) and 9.1 ± 1.0 km (PFISR). Comparison of PFISR and rocket results for the period 12:40:14 UT to 12:55:32 UT show excellent agreement in the κ measurements over a limited height range of 108–118 km, although the estimates for z_0 do not agree to within measurement uncertainties.

[31] 5. Measurements of the κ scale height agree well with neutral atmosphere scale height measurements from an ionization gauge (IG) on the same rocket between 118 km and 125 km (Figure 9). To within measurement uncertainties, the κ scale height is relatively constant between 118 and 130 km, significantly below the IG measurements at altitudes above 125 km.

[32] 6. Variability in κ for a single rocket, between rockets flown 16 min apart, and between in situ and ground-based observations, is evidence for substantial structuring of the atmospheric neutral density vertically and/or horizontally. This structure is suggestive of structured frictional heating at scales of 1–10 km. Such variations in space and time may account for the underestimate in z_0 by PFISR during the interval 12:24:54 UT to 12:40:13 UT.

[33] 7. Qualitatively, MSIS and IRI models perform well in representing collision frequencies under relatively quiet auroral conditions, but there are disparities between the empirical models and observations over scales of 1–10 km (Figures 8a and 8b).

[34] 8. There were no indications of significant structure at scales below 1 km in either ion density or ion temperature between altitudes of 118 km and 135 km (Figure 6).

Appendix A

A1. Uncertainty in κ (in Situ Technique)

[35] We estimate the uncertainty in κ at a given height from

$$\Delta\kappa = \frac{\mathrm{d}\kappa}{\mathrm{d}\theta}\Delta\theta, \tag{A1}$$

where θ is the deflection of the ram velocity vector from the direction it would have if the plasma were collisionless. The uncertainty in this angle, $\Delta\theta$, has two parts,

$$\Delta\theta = \sqrt{(\Delta\theta_\mathrm{m})^2 + (\Delta\theta_\mathrm{e})^2}, \tag{A2}$$

where the measured uncertainty is the error in the observed ram direction and the expected uncertainty is the error in the expected angle, which is derived from the field and neutral wind uncertainties using

$$\Delta\theta_\mathrm{e} = \sqrt{\left(\frac{\partial\theta_\mathrm{e}}{\partial E_x}\Delta E_x\right)^2 + \left(\frac{\partial\theta_\mathrm{e}}{\partial E_y}\Delta E_y\right)^2 + \left(\frac{\partial\theta_\mathrm{e}}{\partial u_x}\Delta u_x\right)^2 + \left(\frac{\partial\theta_\mathrm{e}}{\partial u_y}\Delta u_y\right)^2}$$

where the partial derivatives can be derived from the angle between $\vec{v}_i'$ and $\vec{v}_{E\times B}'$ (Figure 5). Uncertainties in each component of the neutral velocity vector are on the order of 1–5 m s^{-1} over the course of the ten minute observation period. Uncertainties in the electric field components are of order 0.5 mV/m.

A2. Collision Frequency Calculation

[36] The momentum transfer collision frequency height profile is calculated using the NRL-MSISE-00 model mass densities for O, N_2, and O_2, and the dominant IRI ions. The A_p and $F_{10.7}$ averages for the period leading up to the flight are included in the model. The collision frequencies are obtained for all pairs of ion-neutral interactions from the polarization attraction collision frequency from equation (4.88) of *Schunk and Nagy* [2009]. Total collision frequencies between an ion and all other neutral species are obtained from a sum over all neutrals, and the average momentum transfer collision frequency is a density-weighted average of the total collision frequencies for all ions. Relative ion concentrations for NO^+, O_2^+, and O^+ are obtained from IRI 2007. All other IRI species have negligible concentrations at these altitudes. Uncertainties in the calculated collision frequencies can arise from uncertainties in ion or neutral concentration, and ion or neutral temperature. Neutral temperature is obtained from NRL-MSISE-00, and the ion temperature is assumed to be equal to the neutral temperature, which is justified given that the electric fields on the downleg were less than 5 mV m^{-1}.

[37] **Acknowledgments.** This research was supported by the Canadian Space Agency and the Natural Sciences and Engineering Research Council of Canada. Joule II SII development was supported by a contract from the Canadian Space Agency. The authors acknowledge the contributions and expertise of the SII development team, R. B. Hriskevich, J. T. Forshaw, R. M. Thomson, J. G. Aase, and E. P. King, and of the Joule II payload team at the NASA Wallops Flight Facility. PFISR data and collection and analysis was supported by NSF cooperative agreement ATM-0608577, and work at SRI International was supported by NSF grant ATM-0719808. MFL was partially supported under NASA grant NNX07AJ99G and NSF grant AGS-1007539. JKB appreciates valuable discussions with B. Jackel, R. Schunk and J.-P. St.-Maurice.

[38] Robert Lysak thanks the reviewers for their assistance in evaluating this paper.

References

Alcaydé, D., P. Bauer, C. Jaeck, and J. L. Falin (1972), Latitudinal diurnal variation of some atmospheric parameters determined by a simultaneous analysis of incoherent-scatter and satellite-drag data, *J. Geophys. Res.*, *77*, 2368–2376, doi:10.1029/JA077i013p02368.

Bayard, R. T., and D. Alpert (1950), Extension of the low pressure range of the ionization gauge, *Rev. Sci. Instrum.*, *21*(6), 571–572.

Bilitza, D., and B. W. Reinisch (2008), International reference ionosphere 2007: Improvements and new parameters, *Adv. Space Res.*, *42*(4), 599–609, doi:10.1016/j.asr.2007.07.048.

Burchill, J. K., D. J. Knudsen, J. H. Clemmons, K. Oksavik, R. F. Pfaff, C. T. Steigies, A. W. Yau, and T. K. Yeoman (2010), Thermal ion upflow in the cusp ionosphere and its dependence on soft electron energy flux, *J. Geophys. Res.*, *115*, A05206, doi:10.1029/2009JA015006.

Clemmons, J. H., J. H. Hecht, D. R. Salem, and D. J. Strickland (2008), Thermospheric density in the Earth's magnetic cusp as observed by the Streak mission, *Geophys. Res. Lett.*, *35*, L24103, doi:10.1029/2008GL035972.

Davies, J. A., M. Lester, and T. R. Robinson (1997), Deriving the normalised ion-neutral collision frequency from EISCAT observations, *Ann. Geophys.*, *15*, 1557–1569.

Dougherty, J. P., and D. T. Farley (1963), A theory of incoherent scattering of radio waves by a plasma: 3. Scattering in a partly ionized gas, *J. Geophys. Res.*, *68*(19), 5473–5485.

Drakou, E., A. W. Yau, and T. Abe (1997), Ion temperature measurements from the Akebono suprathermal mass spectrometer: Application to the polar wind, *J. Geophys. Res.*, *102*, 17,523–17,540, doi:10.1029/97JA00099.

Emery, B. A., R. G. Roble, N. W. Spencer, L. H. Brace, and M. Sugiura (1985), Thermospheric and ionospheric structure of the Southern Hemisphere polar cap on October 21, 1981, as determined from Dynamics Explorer 2 satellite data, *J. Geophys. Res.*, *90*, 6553–6566, doi:10.1029/JA090iA07p06553.

Finlay, C. C., et al. (2010), International Geomagnetic Reference Field: The eleventh generation, *Geophys. J. Int.*, *183*, 1216–1230, doi:10.1111/j.1365-246X.2010.04804.x.

Heelis, R. A. (1987), Electrodynamics and plasma processes in the ionosphere, *Rev. Geophys.*, *25*, 419–431, doi:10.1029/RG025i003p00419.

Heinselman, C. J., and M. J. Nicolls (2008), A Bayesian approach to electric field and *E*-region neutral wind estimation with the Poker Flat Advanced Modular Incoherent Scatter Radar, *Radio Sci.*, *43*, RS5013, doi:10.1029/2007RS003805.

Horowitz, R., and H. E. LaGow (1957), Upper air pressure and density measurements from 90 to 220 kilometers with the Viking-7 rocket, *J. Geophys. Res.*, *62*(1), 57–78.

Hysell, D. L., G. Michhue, M. F. Larsen, R. Pfaff, M. Nicolls, C. Heinselman, and H. Bahcivan (2008), Imaging radar observations of Farley Buneman waves during the JOULE II experiment, *Ann. Geophys.*, *26*(7), 1837–1850, doi:10.5194/angeo-26-1837-2008.

Hysell, D. L., G. Michhue, M. J. Nicolls, C. J. Heinselman, and M. F. Larsen (2009), Assessing auroral electric field variance with coherent and incoherent scatter radar, *J. Atmos. Sol. Terr. Phys.*, *71*, 697–707, doi:10.1016/j.jastp.2008.10.013.

Knowles, S. H., J. M. Picone, S. E. Thonnard, and A. C. Nicholas (2001), The effect of atmospheric drag on satellite orbits during the Bastille Day event, *Sol. Phys.*, *204*, 387–397, doi:10.1023/A:1014223807360.

Knudsen, D. J., and J. Wahlund (1998), Core ion flux bursts within solitary kinetic Alfvén waves, *J. Geophys. Res.*, *103*(A3), 4157–4169.

Knudsen, D. J., J. K. Burchill, K. Berg, G. A. Enno, C. G. Marcellus, E. P. King, I. Wevers, and R. A. King (2003), A low-energy charged particle distribution imager with a compact sensor for space applications, *Rev. Sci. Instrum.*, *74*, 202–211, doi:10.1063/1.1525869.

Lühr, H., M. Rother, W. Köhler, P. Ritter, and L. Grunwaldt (2004), Thermospheric up-welling in the cusp region: Evidence from CHAMP observations, *Geophys. Res. Lett.*, *31*, L06805, doi:10.1029/2003GL019314.

Nygren, T. (1996), Studies of the E-region ion-neutral collision frequency using the EISCAT incoherent scatter radar, *Adv. Space Res.*, *18*(3), 79–82.

Nygren, T., L. Jalonen, and A. Huuskonen (1987), A new method of measuring the ion-neutral collision frequency using incoherent scatter radar, *Planet. Space Sci.*, *35*(3), 337–343.

Nygren, T., B. S. Lanchester, L. Jalonen, and A. Huuskonen (1989), A method for determining the ion-neutral collision frequency using radar measurements of ion velocity in two directions, *Planet. Space Sci.*, *37*, 493–502.

Picone, J. M., A. E. Hedin, D. P. Drob, and A. C. Aikin (2002), NRLMSISE-00 empirical model of the atmosphere: Statistical comparisons and scientific issues, *J. Geophys. Res.*, *107*(A12), 1468, doi:10.1029/2002JA009430.

Prölss, G. W. (2008), Perturbations of the upper atmosphere in the cleft region, *J. Atmos. Sol. Terr. Phys.*, *70*, 2374–2380, doi:10.1016/j.jastp.2008.06.017.

Reese, K. W., R. M. Johnson, and T. L. Killeen (1991), Lower thermospheric neutral densities determined from Sondre Stromfjord incoherent scatter radar during LTCS 1, *J. Geophys. Res.*, *96*(A2), 1091–1098.

Ritter, P., H. Luehr, and E. Doornbos (2010), Substorm-related thermospheric density and wind disturbances derived from CHAMP observations, *Ann. Geophys.*, *28*(6), 1207–1220, doi:10.5194/angeo-28-1207-2010.

Saint-Maurice, J.-P., and W. B. Hanson (1982), Ion frictional heating at high latitudes and its possible use for an in situ determination of neutral thermospheric winds and temperatures, *J. Geophys. Res.*, *87*, 7580–7602, doi:10.1029/JA087iA09p07580.

Sakanoi, T., H. Fukunishi, K. Igarashi, S. Okano, and N. Nishitani (2009), Neutral-ion interaction in the auroral *E* region obtained from coordinated Fabry-Perot imager and VHF radar observations, *J. Geophys. Res.*, *114*, A09305, doi:10.1029/2008JA013956.

Sangalli, L., D. J. Knudsen, M. F. Larsen, T. Zhan, R. F. Pfaff, and D. Rowland (2009), Rocket-based measurements of ion velocity, neutral wind, and electric field in the collisional transition region of the auroral ionosphere, *J. Geophys. Res.*, *114*, A04306, doi:10.1029/2008JA013757.

Schunk, R., and A. Nagy (2009), *Ionospheres: Physics, Plasma Physics, and Chemistry*, Cambridge Univ. Press, Cambridge, U. K.

St.-Maurice, J. P., K. Schlegel, and P. M. Banks (1981), Anomalous heating of the polar *E* region by unstable plasma waves: 2. Theory, *J. Geophys. Res.*, *86*(A3), 1453–1462.

Storz, M., B. Bowman, M. Branson, S. Casali, and W. Tobiska (2005), High accuracy satellite drag model (HASDM), in *Space Weather*, *Adv. Space Res.*, *36*, 2497–2505, doi:10.1016/j.asr.2004.02.020.

Thayer, J. P. (2000), High-latitude currents and their energy exchange with the ionosphere-thermosphere system, *J. Geophys. Res.*, *105*(A10), 23,015–23,024.

Watanabe, S., B. A. Whalen, D. D. Wallis, and R. F. Pfaff (1991), Observations of ion-neutral collisional effects in the auroral E region, *J. Geophys. Res.*, *96*, 9761–9771, doi:10.1029/91JA00561.

J. K. Burchill and D. J. Knudsen, Department of Physics and Astronomy, University of Calgary, 2500 University Dr., NW, Calgary, AB T2N 1N4, Canada. (burchill@phys.ucalgary.ca)

J. H. Clemmons, Space Science Applications Laboratory, The Aerospace Corporation, 2310 El Segundo Blvd., El Segundo, CA 90245-4691, USA.

M. Larsen, Department of Physics and Astronomy, Clemson University, Clemson, SC 29634, USA.

M. Nicolls, Center for Geospace Studies, SRI International, 333 Ravenswood Ave., Menlo Park, CA 94025-0000, USA.

R. F. Pfaff, NASA Goddard Space Flight Center, Mail Code 612.3, Greenbelt, MD 20771, USA.

D. Rowland, NASA Goddard Space Flight Center, Mail Code 674, Greenbelt, MD 20771, USA.

L. Sangalli, Department of Physics, Royal Military College of Canada, PO Box 1700, Station Forces, Kingston, ON K7K 7B4, Canada.